Thermo-acoustic random response of temperature-dependent functionally graded material panels

ARTICLE *in* COMPUTATIONAL MECHANICS · AUGUST 2010

Impact Factor: 2.53 · DOI: 10.1007/s00466-010-0477-1

4 AUTHORS, INCLUDING:

Mohammad Tawfik
Cairo University
47 PUBLICATIONS **227** CITATIONS

SEE PROFILE

Comput Mech (2010) 46:377–386
DOI 10.1007/s00466-010-0477-1

ORIGINAL PAPER

Thermo-acoustic random response of temperature-dependent functionally graded material panels

Hesham Hamed Ibrahim · Hong Hee Yoo · Mohammad Tawfik · Kwan-Soo Lee

Received: 24 December 2008 / Accepted: 27 January 2010 / Published online: 19 February 2010

Abstract A nonlinear finite element model is provided for the nonlinear random response of functionally graded material panels subject to combined thermal and random acoustic loads. Material properties are assumed to be temperature-dependent, and graded in the thickness direction according to a simple power law distribution in terms of the volume fractions of the constituents. The governing equations are derived using the first-order shear-deformable plate theory with von Karman geometric nonlinearity and the principle of virtual work. The thermal load is assumed to be steady state constant temperature distribution, and the acoustic excitation is considered to be a stationary white-Gaussian random pressure with zero mean and uniform magnitude over the plate surface. The governing equations are transformed to modal coordinates to reduce the computational efforts. Newton–Raphson iteration method is employed to obtain the dynamic response at each time step of the Newmark implicit scheme for numerical integration. Finally, numerical results are provided to study the effects of volume fraction exponent, temperature rise, and the sound pressure level on the panel response.

H. H. Ibrahim · H. H. Yoo · K.-S. Lee
Department of Mechanical Engineering, Hanyang University, Seoul 133-791, South Korea

H. H. Yoo
e-mail: hhyoo@hanyang.ac.kr

K.-S. Lee
e-mail: ksleehy@hanyang.ac.kr

H. H. Ibrahim (✉)
Space Division, National Authority for Remote Sensing and Space Sciences, Cairo 11769, Egypt
e-mail: hesham.ibrahim@narss.sci.eg

M. Tawfik
Aerospace Engineering Department, Cairo University, Giza, Egypt
e-mail: mohammad.tawfik@gmail.com

Keywords Functionally graded materials · Thermoacoustic vibration · Nonlinear FEM

1 Introduction

Functionally graded materials (FGMs) are non-homogeneous composites characterized by a smooth and continuous change of material properties from one surface to the other. This is achieved by gradually varying the volume fraction of the constituent materials. Functionally graded materials are usually composed of two or more materials whose volume fractions are changing smoothly and continuously along desired direction(s). This continuous change in the compositions leads to a smooth change in the mechanical properties, which has many advantages over the laminated composites, where the delamination and cracks are most likely to initiate at the interfaces due to the abrupt variation in the mechanical properties between laminas. One of the advantages of using these materials is that they can survive environments with high temperature gradients, while maintaining structural integrity. Accordingly, one of the most important applications of FGMs is in the skin panels of supersonic and hypersonic flight vehicles, which have to survive the harsh thermal and mechanical loadings.

Thin plates are a commonly used form of structural components especially in aerospace vehicles, such as high-speed aircraft, rockets, and spacecrafts, which are subjected to thermal loads due to aerodynamic and/or solar radiation heating, and random acoustic loads due to engine and/or aerodynamic transonic noise. This results in a temperature and pressure distributions over the panel surface. The presence of these thermal field may cause large thermal deflections (thermal buckling) of the skin panels, which could affect the dynamic response of such panels. Accordingly, when

studying the acoustic response of skin panels, it is important to consider the interactive effect of thermal and acoustic loads.

A literature review on the nonlinear response and sonic fatigue of surface panels was presented by Vaicaitis [1]. Experiments were performed to study thermally loaded panels under random excitation by Istenes et al.[2], Ng and Clevenson [3] and Murphy et al. [4], where a snap-through phenomenon and frequency shifting due to nonlinear large amplitude vibration were observed. Locke [5] investigated the large deflection random vibration of a thermally buckled thin isotropic plate, using the method of equivalent linearization, while assuming temperature-independent material properties. Abdel-Motagaly et al. [6] utilized the finite element numerical integration to study the nonlinear panel response under combined aerodynamic and acoustic loads. Dhainaut et al. [7] presented a finite element formulation for the prediction of nonlinear random response of thin isotropic and composite panels subjected to the simultaneous action of high acoustic loads and elevated temperatures. The temperature-dependence of material properties was not taken into consideration in their formulation. Ibrahim et al. [8] provided a time-domain finite element formulation to investigate the nonlinear random response of composite plates impregnated with pre-strained SMA fibers subject to thermal and random acoustic loads.

Extensive research work has been carried out on the FGM since its concept was proposed in the late 1980s. Reddy [9] developed both theoretical and finite element formulations for thick FGM plates according to the Higher-order Shear Deformation Plate Theory, and studied the non-linear dynamic response of FGM plates subjected a suddenly applied uniform pressure. El-Abbassi and Meguid [10] provided a new thick shallow shell element to study the thermoelastic behavior of functionally graded structures made of shells and plates. The element accounts for the varying elastic and thermal properties across its thickness. Zenkour [11] presented a new generalized shear deformation theory to study the static response for a simply supported functionally graded rectangular plate subjected to a transverse uniform load. Dai et al. [12] developed a mesh free model for the active shape control and the dynamic response suppression of a FGM plate containing piezoelectric sensors and actuators. Batra and Jin [13] adopted the first-order shear deformation theory coupled with finite element method to study the vibration of functionally graded anisotropic rectangular plate with different edge support conditions. The functional grading was achieved through continuously changing the fiber orientation angle through the thickness. Kim [14] developed an analytical technique to investigate the effect of temperature on the vibration characteristics of thick functionally graded rectangular plates, taking into account the temperature-dependence of the material properties. The influence of thermal environment on the critical flutter dynamic pressure of a flat FGM panel was studied by Prakash and Ganapathi [15]. Ibrahim et al. [16] developed a frequency-domain solution to predict the flutter limit-cycle oscillation amplitudes of FGM panels under combined aerodynamic and thermal loads. To account for the temperature-dependence of material properties, the thermal strain was modeled as an integral quantity of thermal expansion coefficient with respect to temperature. Ibrahim et al. [17] extended the formulation presented in [16] by including the shear deformation effect to make it capable of handling thick FGM panels. Sohn and Kim [18] studied the static and dynamic stabilities of FGM panels under supersonic airflows and elevated temperatures environment, while assuming temperature-independent material properties.

This article extends the formulation presented by Ibrahim et al. [8], to make it able to handle non-symmetric materials such as FGMs. This is achieved by adding the effect of the bending-extension coupling, i.e., by assuming that the bending-extension coupling matrix $[\mathbf{B}] \neq 0$. Moreover, to the best of authors' knowledge, the combined effect of thermal and acoustic loads on the nonlinear vibration response of *thick* FGM panels has not been yet accomplished in the literature. As the use of panels made of FGMs is expected to increase, it is worth investigating the response of such panels under combined thermal and random acoustic loads. In this work, a time-domain solution is developed for the nonlinear vibration response of thick FGM panels under combined thermal, and random acoustic loads. A nonlinear finite element model is provided based on the first-order shear-deformable plate theory with von Karman geometric nonlinearity and the principle of virtual work. Material properties are assumed to be temperature-dependent, and graded in the thickness direction according to a simple power law distribution in terms of the volume fractions of the constituents. Newton–Raphson iteration method is employed to obtain the dynamic response at each time step of the Newmark implicit numerical integration scheme. Finally, numerical results are provided to study the effects of volume fraction exponent, temperature rise, and the sound pressure level (SPL) on the panel response.

2 Finite element formulation

2.1 Nonlinear strain–displacement relations

The nodal degrees of freedom vector of a nine-noded rectangular element having 5 degrees of freedom at each node can be written as:

$$\{\theta\} = \left\{\{w_b\}, \left\{\phi_x, \phi_y\right\}, \{u, v\}\right\}^T = \left\{\begin{matrix}\{w_b\}\\ \{w_\phi\}\\ \{w_m\}\end{matrix}\right\} = \left\{\begin{matrix}\{w_B\}\\ \{w_m\}\end{matrix}\right\} \quad (1)$$

where w_b is the transverse displacement of the middle plane, ϕ_x and ϕ_y are rotations of the transverse normal about the x and y axes respectively, u and v are the membrane displacements in the x and y directions respectively. Inplane strains and curvatures, based on von Karman's moderately large deflection and first-order shear deformable plate theory, are given by [19]:

$$\begin{aligned}\begin{Bmatrix}\varepsilon_x\\ \varepsilon_y\\ \gamma_{xy}\end{Bmatrix} &= \begin{Bmatrix}\frac{\partial u}{\partial x}\\ \frac{\partial v}{\partial y}\\ \frac{\partial u}{\partial y}+\frac{\partial v}{\partial x}\end{Bmatrix} + \begin{Bmatrix}\frac{1}{2}\left(\frac{\partial w}{\partial x}\right)^2\\ \frac{1}{2}\left(\frac{\partial w}{\partial y}\right)^2\\ \frac{\partial w}{\partial x}\frac{\partial w}{\partial y}\end{Bmatrix}\\ &\quad + z\begin{Bmatrix}\frac{\partial \phi_y}{\partial x}\\ \frac{\partial \phi_x}{\partial y}\\ \frac{\partial \phi_y}{\partial y}+\frac{\partial \phi_x}{\partial x}\end{Bmatrix}\\ &= \{\varepsilon_m\}+\{\varepsilon_\theta\}+z\{\kappa\}\end{aligned} \tag{2}$$

where $\{\varepsilon_m\}$, $\{\varepsilon_\theta\}$, and $z\{\kappa\}$ are the membrane linear strain vector, the membrane nonlinear strain vector, and the bending strain vector, respectively, while the transverse shear strain vector can be expressed as [19]:

$$\begin{Bmatrix}\gamma_{yz}\\ \gamma_{xz}\end{Bmatrix} = \begin{Bmatrix}\phi_x\\ \phi_y\end{Bmatrix} + \begin{Bmatrix}\frac{\partial w}{\partial y}\\ \frac{\partial w}{\partial x}\end{Bmatrix} \tag{3}$$

2.2 Functionally graded materials

Typically, the FGMs are made of a mixture of two materials; a ceramic, which is capable of withstanding high temperature environments due to its low thermal conductivity and a metal which act as a structural element to support loading and prevent fractures. Without losing generality, it is usually assumed that the top surface of an FGM plate is ceramic rich and the bottom is metal rich. The region between the two surfaces consists of a blend of the two materials which is assumed in the form of a simple power law distribution as [12]:

$$P_e(z) = P_C V_C + P_M(1 - V_C) \tag{4}$$

$$V_C = \left(0.5 + \frac{z}{h}\right)^n, \quad (-h/2 \le z \le h/2, 0 \le n \le \infty) \tag{5}$$

where z is coordinate in the thickness direction of a plate; (P_e, P_C, P_M) are effective material properties of the FGM, the properties of the ceramic and the properties of the metal respectively. V_C is the ceramic volume fraction, h is the panel thickness, and power n is the volume fraction exponent.

2.3 Stress–strain relationship of an FGM panel

The relationship of inplane forces $\{N\}$ and bending moments $\{M\}$ in terms of the strain vectors can be written as [17]:

$$\{N\} = [A]\{\varepsilon_m + \varepsilon_\theta\} + [B]\{\kappa\} - \{N_T\} \tag{6}$$

$$\{M\} = [B]\{\varepsilon_m + \varepsilon_\theta\} + [D]\{\kappa\} - \{M_T\} \tag{7}$$

$$\{R\} = \begin{Bmatrix}R_{yz}\\ R_{xz}\end{Bmatrix} = \begin{bmatrix}A_{44} & A_{45}\\ A_{45} & A_{55}\end{bmatrix}\begin{Bmatrix}\gamma_{yz}\\ \gamma_{xz}\end{Bmatrix} = [A^s]\gamma \tag{8}$$

where

$$([A],[B],[D]) = \int_{-h/2}^{h/2}(1, z, z^2)[Q(z,T,n)]\,dz$$

$$[Q(z,T,n)] = \begin{bmatrix}\frac{E(z,T,n)}{1-\nu^2(z,n)} & \frac{\nu E(z,T,n)}{1-\nu^2(z,n)} & 0\\ \frac{\nu E(z,T,n)}{1-\nu^2(z,n)} & \frac{E(z,T,n)}{1-\nu^2(z,n)} & 0\\ 0 & 0 & \frac{E(z,T,n)}{2(1+\nu(z,n))}\end{bmatrix}$$

$$\begin{Bmatrix}N_T\\ M_T\end{Bmatrix} = \int_{-h/2}^{h/2}\left[\left(\int_{T_{ref}}^{T}[Q(z,\tau,n)]\{\alpha(z,\tau,n)\}\,d\tau\right)\right] \times \begin{Bmatrix}1\\ z\end{Bmatrix} dz$$

where $[A]$, $[B]$ and $[D]$ are the extensional stiffness matrix, extensional-bending coupling stiffness matrix and flexural stiffness matrix, respectively. T denotes the temperature, while a constant temperature distribution in the x, y and z directions are assumed. In addition, α denotes the thermal expansion coefficient.

2.4 Acoustic load simulation

The acoustic excitation is assumed as a stationary white-Gaussian random pressure with zero mean and uniform magnitude over the panel surface. Noting that, for the finite element time domain integration method presented in this study, there is no limitation on the random input excitation. It can be stationary or non-stationary and Gaussian or non-Gaussian, as long as a time history for the random excitation is available. The cross-spectral density function S_p of a truncated white-Gaussian pressure uniformly distributed over the panel surface can be given as [7]:

$$S_p = \begin{cases}S_0 = p_o^2 10^{\mathrm{SPL}/10}, & 0 \le f \le f_u\\ 0, & f < 0 \text{ or } f > fu\end{cases} \tag{9}$$

where S_o is a constant, p_o is a reference pressure, $p_o = 20\,\mu$Pa, SPL is sound pressure level in decibels, and f_u is the upper cut-off frequency in Hz. Utilizing Matlab, the Gaussian random pressure $p(t)$ with zero mean and power PW is

expressed as:

$$p(t) = sqrt\,(PW)\,.randn\,([n, 1]) \tag{10}$$

where *randn* is Gaussian random number generation function, n is the amount of numbers need to be generated. For numerical integration, it is equal to the time duration divided by the time step. The power can be calculated from spectrum density S_o and upper cut-off frequency f_u as:

$$PW = S_o \cdot f_u \tag{11}$$

The cut-off frequency should be selected so that it does not only cover the highest natural frequency in the simulation, but also considers the frequency shifting effect due to the nonlinear large amplitude vibration. Generally speaking, it should be selected at least twice the highest linear frequency of the modes included in the simulation [7].

2.5 Governing equations

By using the principle of virtual work and Eqs. 2, 3, 6, 7 and 8, the nonlinear governing equation can be derived as follows [17]:

$$\delta Work = \delta Work_{\text{int}} - \delta Work_{ext} = 0 \tag{12}$$

The internal virtual work δ Work $_{int}$ can be stated as:

$$\begin{aligned}\delta Work_{\text{int}} &= \int_A \Big(\{\delta(\varepsilon_m + \varepsilon_\theta)\}^T \{N\} \\ &\quad + \{\delta\kappa\}^T\{M\} + \{\delta\gamma\}^T\{R\}\Big)\, dA \\ &= \{\delta\theta\}^T \left([K] - [K_T] + \frac{1}{2}[n1] + \frac{1}{3}[n2]\right) \\ &\quad \times \{\theta\} - \{\delta\theta\}^T\{p_T\}\end{aligned} \tag{13}$$

where $[k]$ and $[k_T]$ are the linear and thermal stiffness matrices; $[n1]$ and $[n2]$ are the first- and second-order nonlinear stiffness matrices, respectively. In addition, $\{p_T\}$ is the thermal load vector. On the other hand, the external virtual work $\delta Work_{ext}$ can be stated as:

$$\begin{aligned}&\delta Work_{ext} \\ &= \int_A \begin{pmatrix} -I_o(\{\delta u\}^T\{\ddot{u}\} + \{\delta v\}^T\{\ddot{v}\} + \{\delta w\}^T\{\ddot{W}\}) \\ -I_2(\{\delta\varphi_x\}^T\{\ddot{\varphi}_x\} + \{\delta\varphi_y\}^T\{\ddot{\varphi}_y\} + \{\delta w\}^T\{p(t)\}) \end{pmatrix} dA \\ &= \{\delta\theta\}^T[m]\{\ddot{\theta}\} + \{\delta\theta\}^T\{p(t)\}\end{aligned} \tag{14}$$

where $(I_o, I_2) = \int_{-h/2}^{h/2} \rho\left(1, z^2\right) dz$ with h denoting the plate thickness, $[m]$ is the mass matrix and $p(t)$ is the acoustic load modeled as a white Gaussian random pressure. By substituting Eqs. 13 and 14 into 12, the system governing equations of motion can be written as follows:

$$\begin{aligned}&\begin{bmatrix} M_B & 0 \\ 0 & M_m \end{bmatrix} \begin{Bmatrix} \ddot{W}_B \\ \ddot{W}_m \end{Bmatrix} \\ &+ \left(\begin{bmatrix} K_B & K_{Bm} \\ K_{mB} & K_m \end{bmatrix} - \begin{bmatrix} K_{TB} & 0 \\ 0 & 0 \end{bmatrix} + \frac{1}{3}\begin{bmatrix} N2_B & 0 \\ 0 & 0 \end{bmatrix} \right. \\ &\left. + \frac{1}{2}\begin{bmatrix} N1_{NmB} + N1_{N\phi B} & N1_{Bm} \\ N1_{mB} & 0 \end{bmatrix} \right) \\ &\times \begin{Bmatrix} W_B \\ W_m \end{Bmatrix} = \begin{Bmatrix} P_B(t) \\ 0 \end{Bmatrix} + \begin{Bmatrix} P_{BT} \\ P_{mT} \end{Bmatrix} = \begin{Bmatrix} P_B \\ P_m \end{Bmatrix}\end{aligned} \tag{15}$$

where subscripts B, m, and T stand for bending, membrane and thermal, respectively. Subscripts N_m and N_ϕ denote inplane and bending forces which are dependent on W_m and W_B, respectively. Note that neglecting the in-plane inertia term M_m in Eq. 14 will not bring significant error, since their natural frequencies are 2–3 orders of magnitude higher than those of bending [6].

3 Solution procedures

In this section, a time domain solution is presented for the nonlinear random response of FGM panels under combined acoustic and thermal loads. Separating the membrane and transverse displacement equations in Eq. 15 results in:

$$\begin{aligned}&[M_B]\ddot{W}_B + \left(\begin{matrix} [K_B] - [K_{TB}] + \frac{1}{2}[N1_{NmB}(\{W_m\})] \\ + \frac{1}{2}[N1_{N\phi B}(\{W_B\})] + \frac{1}{3}[N2_B] \end{matrix} \right)\{W_B\} \\ &+ \left([K_{Bm}] + \frac{1}{2}[N1_{Bm}]\right)\{W_m\} = P_B\end{aligned} \tag{16}$$

$$[K_m]\{W_m\} + \left([K_{mB}] + \frac{1}{2}[N1_{mB}]\right)\{W_B\} = \{P_m\} \tag{17}$$

From Eq. 17, the in-plane displacement vector $\{W_m\}$ can be expressed in terms of the bending displacement vector $\{W_B\}$ as:

$$\begin{aligned}\{W_m\} &= [K_m]^{-1}\{P_m\} - [K_m]^{-1}[K_{mB}]\{W_B\} \\ &\quad -\frac{1}{2}[K_m]^{-1}[N1_{mB}]\{W_B\} \\ &= \{W_m\}_o - \{W_m\}_1 - \{W_m\}_2\end{aligned} \tag{18}$$

where $\{W_m\}_o$ is a constant, $\{W_m\}_1$ and $\{W_m\}_2$ are linearly and quadratically dependent on $\{W_B\}$. Thus, the matrix $[\mathrm{N1}_{NmB}\ (\{W_m\})]$ is evaluated by algebraic sum of three components: $[\mathrm{N1}_{NmB}\ (\{W_m\}_o)]$, $[\mathrm{N1}_{NmB}\ (\{W_m\}_1)]$ and $[\mathrm{N1}_{NmB}\ (\{W_m\}_2)]$, which are independent, linearly and quadratically dependent on $\{W_B\}$, respectively. Substituting Eq. 18 into 16, the system equations of motion can be stated

as a function of $\{W_B\}$ as:

$$[M_B]\{\ddot{W}_B\} + \left([K_B] - [K_{TB}] + \frac{1}{2}[N1_{NmB}(\{W_m\})] + \frac{1}{2}[N1_{N\phi B}(\{W_B\})] + \frac{1}{3}[N2_B]\right)\{W_B\} + ([K_{Bm}] + \frac{1}{2}[N1_{Bm}])\left([K_m]^{-1}\{P_m\} - [K_m]^{-1}[K_{mB}]\{W_B\} - \frac{1}{2}[K_m]^{-1}[N1_{mB}]\{W_B\}\right) = \{P_B\} \quad (19)$$

It can be shown that [20];

$$\frac{1}{2}[N1_{Bm}]\{W_m\}_o = \frac{1}{2}[N1_{NmB}(\{W_m\}_o)]\{W_B\} \quad (20)$$

According to Eq. 20, the system equation of motions can be finally stated as:

$$[M_B]\left\{\ddot{W}_B\right\} + \left([K_B] - [K_{TB}] - [K_{Bm}][K_m]^{-1}[K_{mB}] + \left[N1_{NmB}(\{W_m\}_o)\right]\right)\{W_B\} + \left(\frac{1}{2}\left[N1_{N\phi B}(\{W_B\})\right] - \frac{1}{2}\left[N1_{NmB}(\{W_m\}_1)\right] - \frac{1}{2}[K_{Bm}][K_m]^{-1}[N1_{mB}] - \frac{1}{2}[N1_{Bm}][K_m]^{-1}[K_{mB}]\right)\{W_B\} + \left(\frac{1}{3}[N2_B] - \frac{1}{2}\left[N1_{NmB}(\{W_m\}_2)\right] - \frac{1}{4}[N1_{Bm}][K_m]^{-1} \times [N1_{mB}]\right)\{W_B\} = \{P_B\} - [K_{Bm}][K_m]^{-1}\{P_m\} \quad (21)$$

Equation 21 can be numerically integrated in the structural nodal degrees of freedom. But this approach turns to be computationally expensive. Therefore, an alternative and effective solution procedure is to transform Eq. 21 into modal coordinates using reduced system normal modes by expressing the system bending displacement $\{W_B\}$ as a linear combination of a finite number of normal mode shapes as:

$$\{W_B\} \approx \sum_{r=l}^{n} Q_r\{\phi_r\} = [\Phi]\{Q\} \quad (22)$$

where the rth normal mode $\{\phi_r\}$ and the corresponding natural frequency ω_r are obtained from the linear vibration of the system as:

$$\omega_r^2[M_B]\{\phi_r\} = ([K_B])\{\phi_r\} \quad (23)$$

Accordingly, all the matrices in Eq. 21 are transformed into modal coordinates and it can be written in modal coordinates as:

$$[\bar{M}_B]\{\ddot{Q}\} + 2[\zeta_r f_r][\bar{M}_B]\{\dot{Q}\} + \left([\bar{K}] + [\bar{K}_q] + [\bar{K}_{qq}]\right)\{Q\} = \{\bar{P}_B\} \quad (24)$$

where the modal mass and linear stiffness matrices are given by:

$$\left([\bar{M}_B], [\bar{K}]\right) = [\Phi]^T\left([M_B], [K_{lin}]\right)[\Phi] \quad (25)$$

$$[K_{lin}] = [K_B] - [K_{TB}] - [K_{Bm}][K_m]^{-1}[K_{mB}] + \left[N1_{NmB}(\{W_m\}_o)\right] \quad (26)$$

$$\left\{\bar{P}_B\right\} = [\Phi_B]^T\left(\{P_B\} - [K_{Bm}][K_m]^{-1}\{P_m\}\right) \quad (27)$$

The first and second-order nonlinear modal stiffness matrices are given by:

$$\left[\bar{K}_q\right] = [\Phi]^T\sum_{r=1}^{n} Q_r \times \begin{pmatrix} \frac{1}{2}\left[N1_{N\phi B}(\{W_B\})\right]^{(r)} - \frac{1}{2}\left[N1_{NmB}(\{W_m\}_1)\right]^{(r)} \\ -\frac{1}{2}[K_{Bm}][K_m]^{-1}[N1_{mB}]^{(r)} - \frac{1}{2}[N1_{Bm}]^{(r)}[K_m]^{-1}[K_{mB}] \end{pmatrix}[\Phi] \quad (28)$$

$$\left[\bar{K}_{qq}\right] = [\Phi]^T\sum_{r=1}^{n}\sum_{s=1}^{n} Q_r Q_s \times \begin{pmatrix} \frac{1}{3}[N2_B]^{(rs)} - \frac{1}{2}\left[N1_{NmB}(\{W_m\}_2)\right]^{(rs)} \\ -\frac{1}{4}[N1_{Bm}]^{(r)}[K_m]^{-1}[N1_{mB}]^{(s)} \end{pmatrix}[\Phi] \quad (29)$$

Note that, a modal structural damping matrix $2\,[\zeta_r f_r][M_B]$ has been added to Eq. 24 to account for the structural damping effect on the system [7]. The coefficient ζ_r is the modal damping ratio of the rth mode, while f_r is the rth natural frequency in Hz.

4 Numerical results and discussions

The nonlinear vibration behavior of an FGM panel is investigated with three parameters in the study; volume fraction exponent n, temperature rise ΔT and sound pressure level *SPL*. All panel edges are assumed clamped. A damping ratio that follows the relation $\zeta_r f_r = \zeta_s f_s$ is used with a fundamental modal damping coefficient ζ_1 equal to 0.02. Newmark implicit numerical integration scheme is utilized to solve the system differential equations with a time step equals 1/10000, while Newton–Raphson iteration scheme is adopted to solve the nonlinear algebraic system of equations at each time step [21]. The dimensions of the FGM panel are chosen to be $0.305 \times 0.305 \times 0.002$ (m) as frequently appears in the literature of such field. A uniform temperature rise is applied to the panel. The FGM panel adopted in this study is a mixture of nickel and silicon nitride (Si_3N_4). The properties of the constituent materials are assumed to be temperature-dependent according to the following relation [16]:

$$P = P_o\left(1 + P_1T + P_2T^2 + P_3T^3\right) \quad (30)$$

Table 1 Temperature-dependence coefficients for nickel and silicon nitride

Properties	Material	P_o	P_1	P_2	P_3
E (MPa)	Si_3N_4	348.43e9	−3.07e−4	2.2e−7	−8.9e−11
	Nickel	223.95e9	−2.79e−4	3.9e−9	0
α (1/°C)	Si_3N_4	5.8723e−6	9.09e−4	0	0
	Nickel	9.9209e−6	8.71e−4	0	0
ρ (kg/m^3)	Si_3N_4		2,370		
	Nickel		8,900		
ν	Si_3N_4		0.24		
	Nickel		0.31		

where, the coefficients P_o, P_1, P_2 and P_3 for young's modulus E, the Poisson ratio ν and the thermal expansion coefficient α of nickel and silicon nitride are given in Table 1 [23].

4.1 Validation of the formulation

Accurate nonlinear analytical results and test data for panels under white-Gaussian acoustic pressure and thermal loads are not available in the literature. Validation of the present nonlinear modal formulation will thus consist of two parts: (1) nonlinear free vibrations to assess the accuracy of the homogenous solution of equation, i.e., the accuracy of the left-hand side of Eq. 21, and (2) nonlinear thermal deflection to assess the accuracy of the particular solution of Eq. 21. Both could be accomplished by validating the fundamental frequencies of a thermally post-buckled panel.

Figure 1 shows the variation of fundamental frequency versus temperature for an eight-layered symmetric $[0/45/-45/90]_s$ graphite-epoxy laminate with panel dimensions $0.380 \times 0.305 \times 0.002$ (m). The panel edges are all simply supported which are immovable for the inplane directions. Uniform temperature rise was applied to the panel and the reference temperature was assumed to be 24°C. The results presented in Fig. 1 were compared to those of Fig. 16 in Ref. [24] and were found to be in a good agreement.

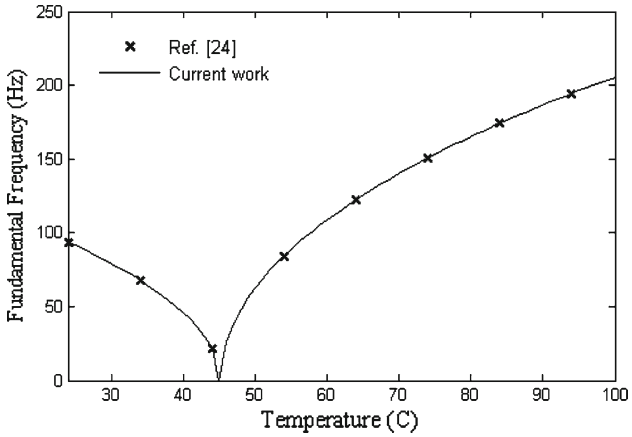

Fig. 1 Variation of the fundamental frequency of a simply supported graphite-epoxy panel versus temperature

4.2 Nonlinear vibration behavior

This section presents the thermo-acoustic response of a clamped FGM panel having $n = 0$ (Si_3N_4), $n = 1$ and $n = \infty$ (nickel), temperature rises (ΔT) = 0, 8, 16 and 24° C, and SPLs = 90, 110 and 130 dB. For a panel under combined thermal and random acoustic loads, three types of motion are expected: (i) linear random vibration about one of the two thermally buckled positions, (ii) snap-through between the two buckled positions, and (iii) nonlinear random vibration over the two thermally buckled positions.

To determine the suitable mesh size and number of normal modes for the current application, a convergence study is depicted in Table 2 for a clamped nickel panel ($n = \infty$) with a temperature rise $\Delta T = 8$°C and sound pressure levels SPL = 90 dB. It is found that using 8×8 mesh (64 elements) and six symmetric normal modes for modal transformation result in a converged solution and thus used, noting that linear normal modes can efficiently express the panel nonlinear response in panels with all edges clamped [22].

The maximum non-dimensional deflection (W_{max}/h) versus time for a panel affected by a SPL = 90 dB is presented in Figs. 2, 3, 4 and 5. The time-history response of a nickel panel is illustrated in Fig. 2. It is seen that at room temperature ($\Delta T = 0$°C), the panel exhibits basically small-deflection random vibration (rms = 0.0018). At $\Delta T = 8$°C, the panel shows a decreased stiffness with such temperature rise through having higher deflection random vibration with rms = 0.0038, which is almost double the room temperature value. At $\Delta T = 16$ and 24°C, which exceed the critical buckling temperature rise of the nickel panel [16], it is found that the thermal post-buckling deflections dominated the response and the panel shows a small-deflection random vibration about the buckling equilibrium position. Figure 3 depicts the central-line vibration mode shape for a nickel panel during certain period of time, while being at $\Delta T = 8$°C and SPL = 90 dB. Due to the uniform distribution of the acoustic

Table 2 Modal and mesh size convergence study

Mesh size	4 × 4 (16 elements)			6 × 6 (36 elements)			8 × 8 (64 elements)		
No. of modes	1	3	6	1	3	6	1	3	6
Deflection root mean square (rms) value	0.0024	0.0022	0.0022	0.0043	0.0038	0.0038	0.0043	0.0038	0.0038

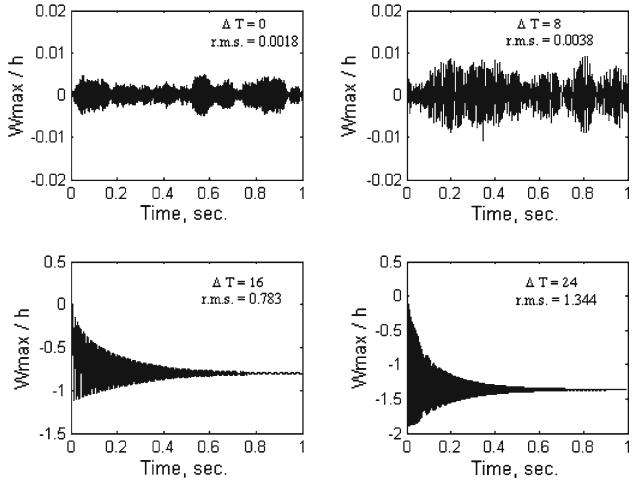

Fig. 2 Time histories for a nickel panel with SPL = 90 dB and at different temperature

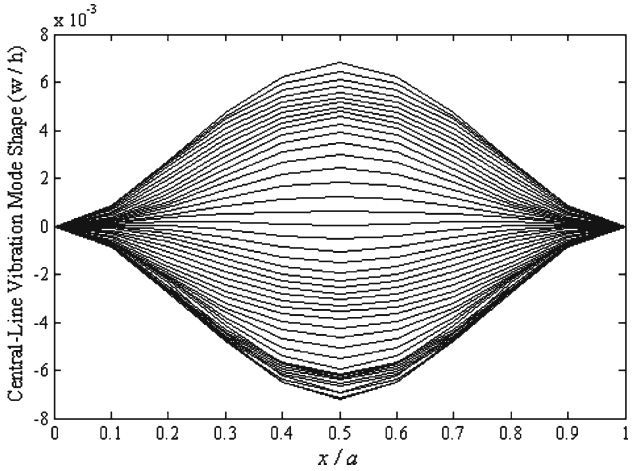

Fig. 3 Central-line vibration mode shape for a nickel panel during certain period of time with SPL = 90 dB and $\Delta T = 8°C$

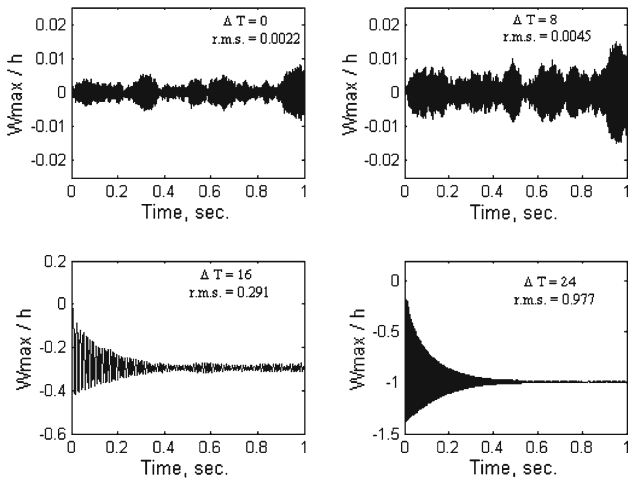

Fig. 4 Time histories for an FGM panel with $n = 1$, SPL = 90 dB and at different temperature rises

pressure, the panel is seen to mainly vibrate in the first mode. For the FGM ($n = 1$) panel shown in Fig. 4, it is seen that the panel experiences higher deflection random vibration at $\Delta T = 0$ and 8°C compared to the nickel panel response presented in Fig. 2. In addition, the FGM ($n = 1$) panel shows lower thermal post-buckling deflections at $\Delta T = 16$ and 24°C compared to the nickel panel resulting in a noticeable reduction in the deflection root mean square values at these temperature rise values which is favorable regarding the aerodynamic performance of such panels. The ceramic panel ($n = 0$) time-history responses presented in Fig. 5 show the highest deflection random vibrations at $\Delta T = 0$ and 16°C, while having the lowest value (rms = 0.535) at $\Delta T = 24°C$. The higher thermal post-buckling deflections of the nickel and FGM panels are not favorable regarding the aerodynamic performance of such panels. But, the nonlinear stiffness added to these panels due thermal deflection is found to weaken the effect of the acoustic pressure, resulting in lower vibration amplitudes about the equilibrium buckling position which may enhance the fatigue-life performance of such panels.

The maximum non-dimensional deflection ($W_{\max}/h$) versus time for a panel affected by a SPL = 110 dB is presented in Figs. 6, 7 and 8. At $\Delta T = 0$ and 8°C, the nickel panel responses presented in Fig. 6 show deflection root mean square values 0.018 and 0.039, which are one order of magnitude higher than those of the 90 dB responses presented in Fig. 2. $\Delta T = 16$ and 24°C, the thermal buckling deflections are found to continue dominating the acoustic pressure showing almost the same deflections root mean square as those of the 90 dB. The FGM ($n = 1$) panel presented in Fig. 7 exhibits the trend shown in Fig. 6 except at $\Delta T = 16°C$, where the acoustic pressure started to overcome the nonlinear stiffness due to thermal bucking showing a small number of snap-through motion between the two buckling equilibrium positions. In addition, at room temperature, the FGM panel

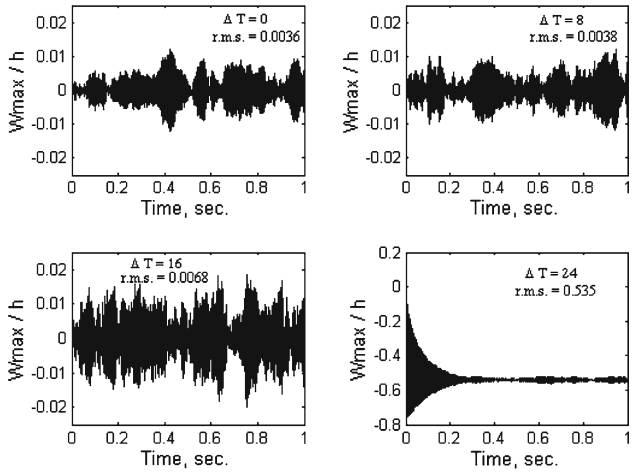

Fig. 5 Time histories for a ceramic (Si_3N_4) panel with SPL = 90 dB and at different temperature rises

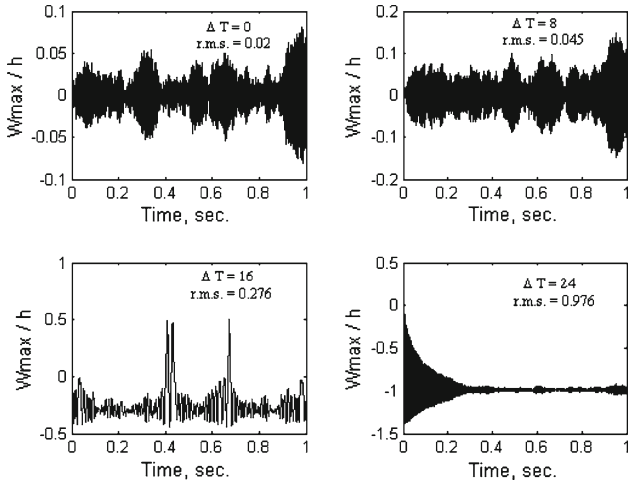

Fig. 7 Time histories for an FGM panel with $n = 1$, SPL = 110 dB and at different temperature rises

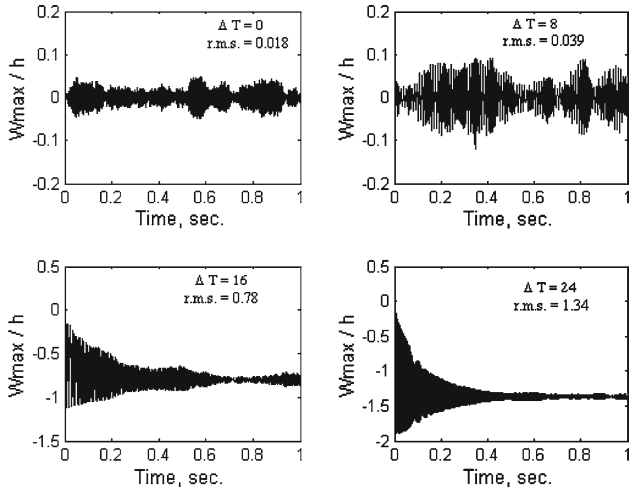

Fig. 6 Time histories for a nickel panel with SPL = 110 dB and at different temperature rises

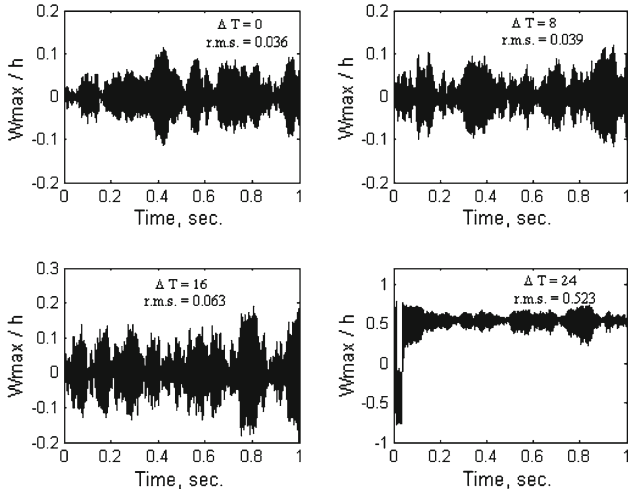

Fig. 8 Time histories for a ceramic (Si_3N_4) panel with SPL = 110 dB and at different temperature rises

shows a response intermediate to the nickel ceramic panels presented in Figs. 6 and 8, respectively.

For the case of a 130-dB sound pressure level, the time-histories responses of an FGM panel having different values of the volume fraction exponent n and at different values of temperature rise are shown in Figs. 9, 10 and 11. The nickel panel presented in Fig. 9 shows a large-amplitude random vibration at $\Delta T = 0$ and 8°C compared to its response at 90 and 110 dB. At $\Delta T = 16$°C, the nonlinear stiffness that comes from thermal deflection is seen to counteract the acoustic pressure resulting in a small-amplitude random vibration about one of the equilibrium buckling positions accompanied by a large number of snap-through motion between the two equilibrium buckling positions. At $\Delta T = 24$°C, the snap-through motion is seen to be completely hindered due to the nonlinear stiffness added to the panel by the increased thermal deflection resulting in a small-amplitude random vibration about the thermally buckled position. According to the time-history responses shown in Fig. 10, a 130-dB random acoustic pressure is found to dominate the FGM panel response resulting in a large-amplitude random vibration up to $\Delta T = 16$°C. For a $\Delta T = 24$°C, the FGM panel exhibits small-amplitude random vibration but the thermally-buckled position accompanied by a weak snap-through motion, while the thermal buckling fails to counteract the acoustic pressure in the ceramic panel response presented in Fig. 11 and the panel shows a large-amplitude nonlinear random vibration over the two thermally buckled positions.

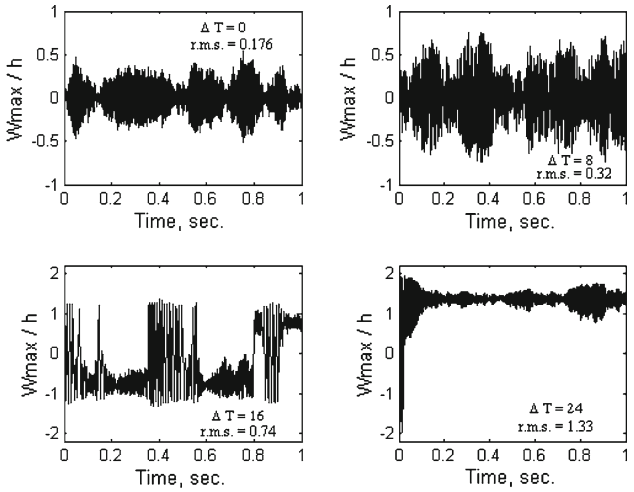

Fig. 9 Time histories for a nickel panel with SPL = 130 dB and at different temperature rises

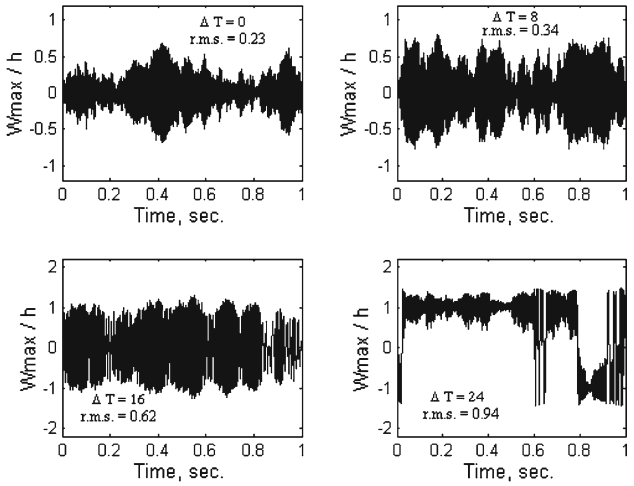

Fig. 10 Time histories for an FGM panel with $n = 1$, SPL = 130 dB and at different temperature rises

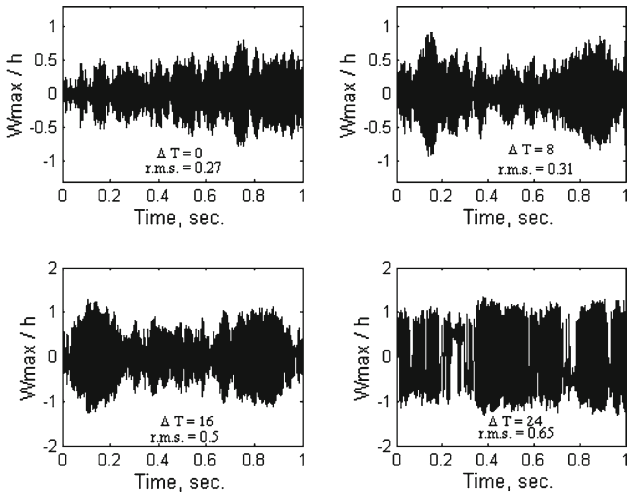

Fig. 11 Time histories for a ceramic (Si_3N_4) panel with SPL = 130 dB and at different temperature rises

5 Conclusion

In this work, a time-domain solution is presented for the nonlinear random response of an FGM panels under combined thermal, and random acoustic loads. A nonlinear finite element model is provided based on the first-order shear-deformable plate theory with von Karman geometric nonlinearity and the principle of virtual work. Material properties are assumed to be temperature-dependent, and graded in the thickness direction according to a simple power law distribution in terms of the volume fractions of the constituents. The acoustic load is assumed to be a white-Gaussian random pressure uniformly distributed over the panel surface. The effects of the volume fraction exponent, temperature rise, and SPL on the nonlinear vibration behavior a clamped FGM panel are studied.

The results showed that, at room temperature, the nickel panel has a better performance regarding the random acoustic response. But, at higher temperatures, it turns to be a matter of compromise between having large thermal post-buckling deflections and hence deterioration in the flight performance, or having higher vibration amplitudes which can affect fatigue life performance. Consequently, overlooking the combined action of the temperature rise and the acoustic noise can lead to inaccuracy in the fatigue life estimation. Finally, it is concluded that for a panel under thermal and random acoustic loads, the FGM panels are not always superior in performance compared to the metal panels.

Acknowledgments This work was supported by the BK21 program, Hanyang University, Seoul, South Korea. The authors wish to express their gratitude for this financial support.

References

1. Vaicaitis R (1994) Nonlinear response and sonic fatigue of national aerospace space plane surface panels. J Aircr 1(1):10–18
2. Istenes RR, Rizzi SA, Wolfe HF (1995) Experimental nonlinear random vibration results of thermally buckled composite panels. In: 36th structures, structural dynamics and materials conference, New Orleans, April 1995, pp 1559–1568
3. Ng CF, Clevenson SA (1991) High-intensity acoustic tests of a thermally stressed plate. J Aircr 28(4):275–281
4. Murphy KD, Virgin LN, Rizzi SA (1996) Characterizing the dynamic response of a thermally loaded acoustically excited plate. J Sound Vib 196(5):635–658
5. Locke JE (1993) Finite element large deflection random response of thermally buckled plates. J Sound Vib 160:301–312
6. Abdel-Motagaly K, Duan B, Mei C (2000) Nonlinear response of composite panels under combined acoustic excitation and aerodynamic pressure. AIAA J 38:1534–1542
7. Dhainaut JM, Gou X, Mei C, Spottswood SM, Wolfe HF (2003) Nonlinear random response of panels in an elevated thermal-acoustic environment. J Aircr 40:683–691
8. Ibrahim HH, Tawfik M, Negm HM (2008) Thermo-acoustic response of shape memory alloy hybrid composite plates. J Aircr 45(3):962–970

9. Reddy JN (2000) Analysis of functionally graded plates. Int J Numer Methods Eng 47:663–684
10. El-Abbasi N, Meguid SA (2000) Finite element modeling of the thermoelastic behavior of functionally graded plates and shells. Int J Comput Eng Sci 1:151–165
11. Zenkour AM (2005) Generalized shear deformation theory for bending analysis of functionally graded plates. J Appl Math Model 30:67–84
12. Dai KY, Liu GR, Han X, Lim KM (2005) Thermomechanical analysis of functionally graded material (FGM) plates using element-free Galerkin method. Comput Struct 83:1487–1502
13. Batra RC, Jin J (2005) Natural frequencies of a functionally graded anisotropic rectangular plate. J Sound Vib 282:509–516
14. Kim YW (2005) Temperature dependent vibration analysis of functionally graded rectangular plates. J Sound Vib 284:531–549
15. Prakash T, Ganapathi M (2006) Supersonic flutter characteristics of functionally graded flat panels including thermal effects. Compos Struct 72:10–18
16. Ibrahim HH, Tawfik M, Al-Ajmi M (2007) Non-linear panel flutter for temperature-dependent functionally graded material panels. Comput Mech 41(2):325–334
17. Ibrahim HH, Tawfik M, Al-Ajmi M (2008) Thermal buckling and nonlinear flutter behavior of functionally graded material panels. J Aircr 44(5):1610–1618
18. Sohn K-J, Kim J-H (2008) Structural stability of functionally graded panels subject to aerothermal loads. Compos Struct 82:317–325
19. Reddy JN (1999) Theory and analysis of elastic plates. Taylor & Francis, Philadelphia
20. Xue DY (1991) Finite element frequency domain solution of nonlinear panel flutter with temperature effects and fatigue life analysis. PhD dissertation, Mechanical Engineering Department, Old Dominion University, Norfolk
21. Bathe KJ (1996) Finite element procedures. Prentice-Hall, Englewood Cliffs
22. Yoo HH (1989) Dynamic modeling of flexible bodies in multibody systems. PhD dissertation, Mechanical Engineering Department, Michigan University, Michigan
23. Touloukian YS (1967) Thermophysical properties of high temperature solid materials. McMillan, New York
24. Park JS, Kim JH, Moon SH (2004) Vibration of thermally post-buckled composite plates embedded with shape memory alloy fibers. Compos Struct 63:179–188